ADVANCED BIOSYSTEMS
www.adv-biosys.com

Photoelectric Silk via Genetic Encoding and Bioassisted Plasmonics

*Jung Woo Leem, Andres E. Llacsahuanga Allcca, Yong Jae Kim, Jongwoo Park, Seong-Wan Kim, Seong-Ryul Kim, WonHyoung Ryu, Yong P. Chen, and Young L. Kim**

Genetically encoded photoelectric silk that can convert photons to electrons (light to electricity) over a wide visible range in a self-power mode is reported. As silk is a versatile host material with electrical conductivity, biocompatibility, and processability, a photoelectric protein is genetically fused with silk by silkworm transgenesis. Specifically, mKate2, which is conventionally known as a far-red fluorescent protein, is used as a photoelectric protein. Characterization of the electrochemical and optical properties of mKate2 silk allows designing a photoelectric measurement system. A series of in situ photocurrent experiments support the sensitive and stable performance of photoelectric conversion. In addition, as a plasmonic nanomaterial with a broad spectral resonance, titanium nitride (TiN) nanoparticles are biologically hybridized into the silk glands, taking full advantage of the silkworms' open circulatory system as well as the absorption band of mKate2 silk. This biological hybridization via direct feeding of TiN nanoparticles further enhances the overall photoelectric conversion ability of mKate2 silk. It is envisioned that the biologically derived photoelectric protein, its ecofriendly scalable production by transgenic silkworms, and the bioassisted plasmonic hybridization can potentially broaden the biomaterial choices for developing next-generation biosensing, retina prosthesis, and neurostimulation applications.

1. Introduction

With the recent advances in implantable biosensors and flexible electronics, there is an ever-growing need for biocompatible or implantable photoelectric materials that convert light to electricity. Retinal prosthesis (or artificial retina), artificial photoreceptors, and neurostimulators are key examples that require such photoelectric conversion devices implanted in the body. Historically, photoelectric effects in rhodopsin (photosensitive receptor protein), bacteriorhodopsin (photosensitive protein found in *Halobacterium*), and chlorophyll were intensively studied to develop bioelectronic devices.[1] Recently, several biomedical photosensors and neural interfaces have been successfully developed using 2D materials (e.g., graphene and molybdenum disulfide) because of the excellent structural and optoelectronic properties.[2] Such materials are known to be biocompatible, but are still exogenous and exotic materials with respect to the human body compositions, most of which are proteins.[3] As a common example, surgical removal of spinal neurostimulator electrodes is often necessary due to infection and allergic inflammation in the surrounding tissue and erosion of the electrodes, putting patients at risk.[4] In this regard, biologically derived biomaterials have the potential for minimizing inflammatory and immune responses in the tissue of the human body.

Dr. J. W. Leem, Prof. Y. L. Kim
Weldon School of Biomedical Engineering
Purdue University
West Lafayette, IN 47907, USA
E-mail: youngkim@purdue.edu
A. E. Llacsahuanga Allcca, Prof. Y. P. Chen
Department of Physics and Astronomy
Purdue University
West Lafayette, IN 47907, USA
Y. J. Kim, Prof. W. Ryu
Department of Mechanical Engineering
Yonsei University
Seoul 03722, Republic of Korea
The ORCID identification number(s) for the author(s) of this article can be found under https://doi.org/10.1002/adbi.202000040.

DOI: 10.1002/adbi.202000040

Dr. J. Park, Dr. S.-W. Kim, Dr. S.-R. Kim
Department of Agricultural Biology
National Institute of Agricultural Sciences
Rural Development Administration
Wanju, Jeollabuk-do 55365, Republic of Korea
Prof. Y. P. Chen
Birck Nanotechnology Center
Purdue University
West Lafayette, IN 47907, USA
Prof. Y. P. Chen, Prof. Y. L. Kim
Purdue Quantum Science and Engineering Institute
Purdue University
West Lafayette, IN 47907, USA
Prof. Y. L. Kim
Purdue University Center for Cancer Research
West Lafayette, IN 47907, USA
Prof. Y. L. Kim
Regenstrief Center for Healthcare Engineering
Purdue University
West Lafayette, IN 47907, USA

One of the best biomaterials found in nature is silk. Primarily, silkworm (*Bombyx mori*) silk is composed of several different proteins, consisting of heavy-chain (molecular weight ≈ 350 kDa) and light-chain (molecular weight ≈ 25 kDa) proteins, and the protein backbone is a repetitive amino acid sequence $(Gly\text{-}Ser\text{-}Gly\text{-}Ala\text{-}Gly\text{-}Ala)_n$.[5] Importantly, silk has significant electrical conductivity when exposed to a humid environment.[6] Water molecules diffuse into the porous matrix of silk fibers, become mobile, and interact with common ions forming elements (i.e., Na, K, Cl, etc.) as well as with the protein matrix, resulting in the generation of ionic mobile charge carriers. As manifested by the silvery and vibrant reflection, light scattering in silk is extremely strong near the Anderson regime,[7] potentially allowing for strong coupling of incident light with light-harvesting devices.[8] Silk produced by silkworms has successfully demonstrated as flexible fabrics by processing silk into a variety of host materials and structures for optics, electronics, biomedicine, and energy harvesting.[9] More importantly, low immunogenicity and biocompatibility of silk are ideal for biomedical applications.[9b] Silkworms can serve as a bioreactor (or) to produce recombinant proteins in a scalable and ecofriendly manner.[10] Then, would it be possible to further realize photoelectric conversion silk?

First, we take inspiration from some fluorescent proteins that can generate reactive oxygen species (ROS) upon visible light illumination.[11] The ROS generation and the photoelectric conversion are two sides of the same coin in terms of redox reactions and electrochemistry; photoinduced electrons are tightly related to the photoelectric conversion property.[12] The phototoxicity and cytotoxicity of some fluorescent proteins (e.g., KillerRed, SuperNova, mKate2, miniSOG, and TagRFP) are well acknowledged and are utilized in different manners.[11] For example, such ROS-generating fluorescent proteins are widely exploited to selectively ablate specific tissue (also known as chromophore-assisted light inactivation).[13] The protein structure for the generation and release of ROS is currently understood such that a cleft-like opening channel filled with water (oxygen) molecules inside a phototoxic fluorescent protein is responsible.[12a,14] Although the exact species of ROS are dependent on the types of photoreactions and the local molecular oxygen environments,[11a] Type I photoreaction in fluorescent proteins is suggested to have long-range electron transfer via quantum mechanics of direct tunneling or hopping.[15] Indeed, there were also successful demonstrations to use green fluorescent proteins (GFP) as an electron donor in photoelectric devices.[16]

Second, transgenic silkworms can be a viable and practical option for cost-effective and scale-up hybridization of silk with the proposed photoelectric fluorescent proteins.[17] Transgenesis of silkworms (*Bombyx mori*) provides high-level expression and efficient production of recombinant proteins of interests. The unique autotomy and physiology of silkworms can be used to biologically hybridize silk with other functional nanomaterials, which can overcome some limitations in biologically derived biomaterials. Due to the open circulatory system of silkworms, nanomaterials fed by oral exposure and intake are diffused to the silk glands, which are the only organ where silk proteins are synthesized and secreted in the silkworm, and nanomaterial-embedded silk fibers can be produced by the silk spinning process.[18] Several different functional nanomaterials (e.g., graphene, carbon nanotube, titanium dioxide, and quantum dot) have recently been incorporated with silk via direct feeding of modified diets to silkworms to produce functionalized silk with superior mechanical, thermal, and electrical properties, ultraviolet protection, or fluorescent colors.[18–19]

In this paper, we report a photoelectric conversion ability of silk genetically fused with a photoelectron-generating fluorescent protein (i.e., monomeric far-red fluorescent protein mKate2 derived from sea anemone *Entacmaea quadricolor*). First, we demonstrate the production of photoelectric silk with mKate2 via silkworm transgenesis using the *piggyBac* transposon method (referred to as mKate2 silk). Second, we characterize the bandgap structure and redox potential of mKate2 silk and design a photoelectric detection platform that can be activated in a broad visible light range. Third, we conduct a series of in situ photocurrent experiments to demonstrate the sensitive and stable photoelectric conversion properties of mKate2 silk under different illumination conditions. Finally, we show that bioassisted hybridization of unconventional plasmonic nanomaterials (i.e., titanium nitride, TiN) into mKate2 silk (referred to as TiN-hybridized mKate2 silk) via direct oral intake enhances the photoelectric conversion performance. This study lays the foundation that photoelectric silk can serve as an alternative photoelectric biomaterial and that transgenic and diet-enhanced silkworms can produce such photoelectric biomaterials in a scalable and eco-friendly manner.

2. Results and Discussion

2.1. Photoelectric Conversion Silk Produced by Silkworm Transgenesis

Figure 1a depicts the overall idea that transgenic silk fused with mKate2 can convert light to electricity by generating photoinducible electrons upon visible light illumination. Here, mKate2, which is a photoelectric protein, is chosen for the enhanced fluorescent properties and photostability.[20] mKate2 is one of the highly phototoxic fluorescent proteins, generating mainly two types (i.e., superoxide anion and singlet oxygen) of ROS resulting from Type I (electron transfer) and Type II (energy transfer) photoreactions.[11a,12d] Far-red wavelength fluorescent proteins are particularly useful for photoelectric conversion in the visible light range. As mKate2 has the emission peak at λ_{em} = 633 nm, the broad absorption range below 633 nm enables for light trapping in the broad visible wavelength range.[20] To genetically hybridize mKate2 and silk, the popular germline *piggyBac* transformation method is used for domesticated silkworms (*Bombyx mori*) (see Experimental Section).[12d,17a,17b] In brief, the transformation vector (p3xP3-EGFP-pFibH-mKate2) for mKate2-expressed silk (Figure 1b), which is constructed by fusing mKate2 gene with N-terminal and C-terminal domains of the fibroin heavy-chain promoter (pFibH) of silk and the vector DNA, is injected with a helper vector into preblastoderm embryos of silkworms. It should be noted that 3xP3-EGFP is served only for screening a large number of G1 broods, because the fluorescent signal of enhanced green fluorescent protein (EGFP) is easily monitored in the stemmata and the nervous

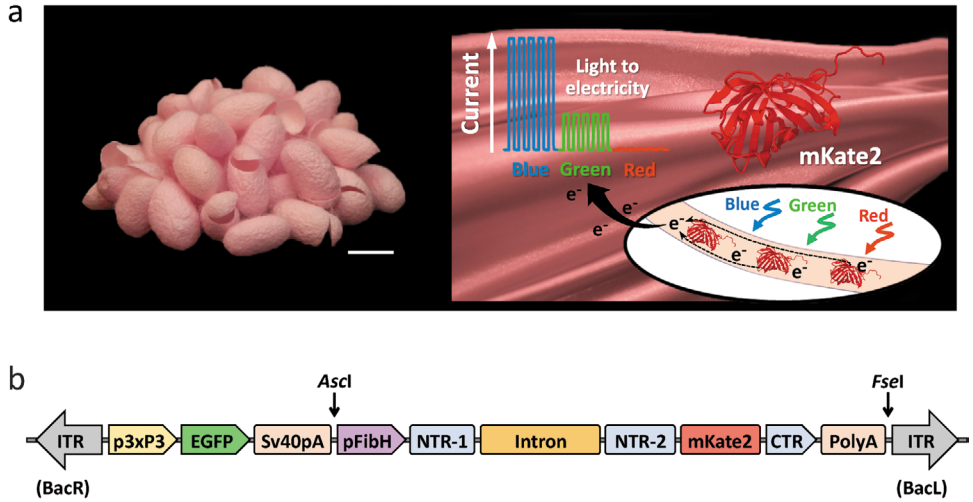

Figure 1. Photoelectric silk via genetically hybridization of a photoelectric fluorescent protein. a) Photograph of mKate2 silk cocoons produced by silkworms genetically engineered using the *piggyBac* transposon method and schematic illustration of photoelectric conversion in transgenic silk genetically hybridized with a photoelectric fluorescent protein (i.e., mKate2). Reacted by light illumination in the visible light, mKate2 silk generates a photocurrent. The scale bar is 2 cm. b) Physical structure of the transformation vector (p3xP3-EGFP-pFibH-mKate2) for mKate2 silk. The *piggyBac* transposon method transposes between vectors and chromosomes via a "cut and paste" approach. pFibH: fibroin heavy chain promoter domain (1124 bp), NTR-1: N-terminal region 1 (142 bp), intron: first intron (871 bp), NTR-2: N-terminal region 2 (417 bp), CTR: C-terminal region (179 bp), PolyA: poly(A) signal region (301 bp), EGFP: enhanced green fluorescent protein gene (720 bp), mKate2: monomeric far-red fluorescent protein (720 bp), ITR: inverted repeat sequences of *piggyBac* arms, 3 × P3: 3 × P3 promoter (273 bp), and Sv40pA: Sv40 polyadenylation signal sequence (268 bp). The restriction enzyme sites for the construction of recombinant vectors are indicated with the arrows.

system at early embryonic and larval stages. In mKate2 silk spun by the transgenic silkworms, the mass density of mKate2/fibroin heavy-chain fusion recombinant protein is estimated to be ≈12.6%.[21] The mKate2 silk cocoons have a reddish-pink color owing to the optical absorption and emission bands of mKate2 (Figure 1a).

2.2. Electrochemical and Optical Properties of mKate2 Silk

With a properly designed electrolytic device, mKate2 silk can possess current–voltage characteristics in a similar manner to photosensors. In particular, the electronic energy level between an electron donor and an electron acceptor plays an important role in electron transport.[12c,22] To characterize the electronic energy level of mKate2 silk and to provide the theoretical foundation for electron transfer in mKate2 silk, we conduct a square wave voltammetry analysis using mKate2 silk (**Figure 2**a; Figure S1, Supporting Information). The first reduction peak is observed at the potential bias of −1.47 V with respect to the silver/silver chloride (Ag/AgCl) reference electrode. The calculated energy level of the lowest unoccupied molecular orbital (LUMO) is −3.18 eV from the first reduction potential, using the empirical relationship of LUMO = $-(E_{red} + 4.65)$ eV with the reduction potential E_{red}. The optical energy bandgap (E_g) of mKate2 silk is estimated to be 2 eV, using $E_g = 1240$ eV/λ_g (i.e., $\lambda_g = 620$ nm in Figure 2b). The resultant energy level of the highest occupied molecular orbital (HOMO) is -5.18 eV. This theoretical estimation provides us with the idea that the energy level of mKate2 silk can be well integrated with titanium dioxide (TiO_2), given that the energy level of the conduction band E_c is −4.2 eV, allowing for effective migration of electrons photogenerated by mKate2 silk (Figure 2c). Fortunately, TiO_2 is readily accessible as one of the common electron acceptors (e.g., anode electrode) in a variety of optoelectronic devices.[23]

To further assert the generation and transport of photoinduced electrons (i.e., charge carriers) by mKate2 silk, we perform a photoluminescent (PL) analysis of mKate2 silk in the presence of TiO_2 nanoparticles (anatase phase and size <25 nm). Because PL emission arises from the recombination of free carriers, PL analyses are useful to investigate the trapping, migration, and recombination processes of photoinduced charge carriers between photosensitizers and metal oxide materials.[12c] In this additional test, TiO_2 nanoparticles are randomly embedded in the fiber network of mKate2 silk cocoon samples (thickness ≈ 250 μm and diameter = 0.5 cm) (see Experimental Section). The concentration of TiO_2 is minimized such that the increase in the reflectance intensity at the excitation wavelength range of λ = 470–550 nm is only 5%, which also confirms no light absorption of TiO_2 at the corresponding wavelengths. The broadband absorption of mKate2 silk (without TiO_2 nanoparticles) in the wavelength range of 400– 620 nm means that it can be excited for photoelectric conversion in the wide visible range (Figure 2b). In the presence of TiO_2 nanoparticles, the PL emission (λ_{em} = 600–800 nm with λ_{ex} = 530 nm) of mKate2 silk is considerably lower with a reduction of 26% in the PL intensity, compared to the bare mKate2 silk sample (without TiO_2) (Figure 2d). This PL quenching indicates that the electrons excited to the LUMO level of mKate2 silk diffuse and reach to TiO_2 nanoparticles.[12c,16a] Thus, the electrochemical and optical properties of mKate2 silk support the idea that transgenic mKate2 silk can be used as a photoelectron-generating biomaterial, which could also be mass-produced by the bioreactor (i.e., silkworms).

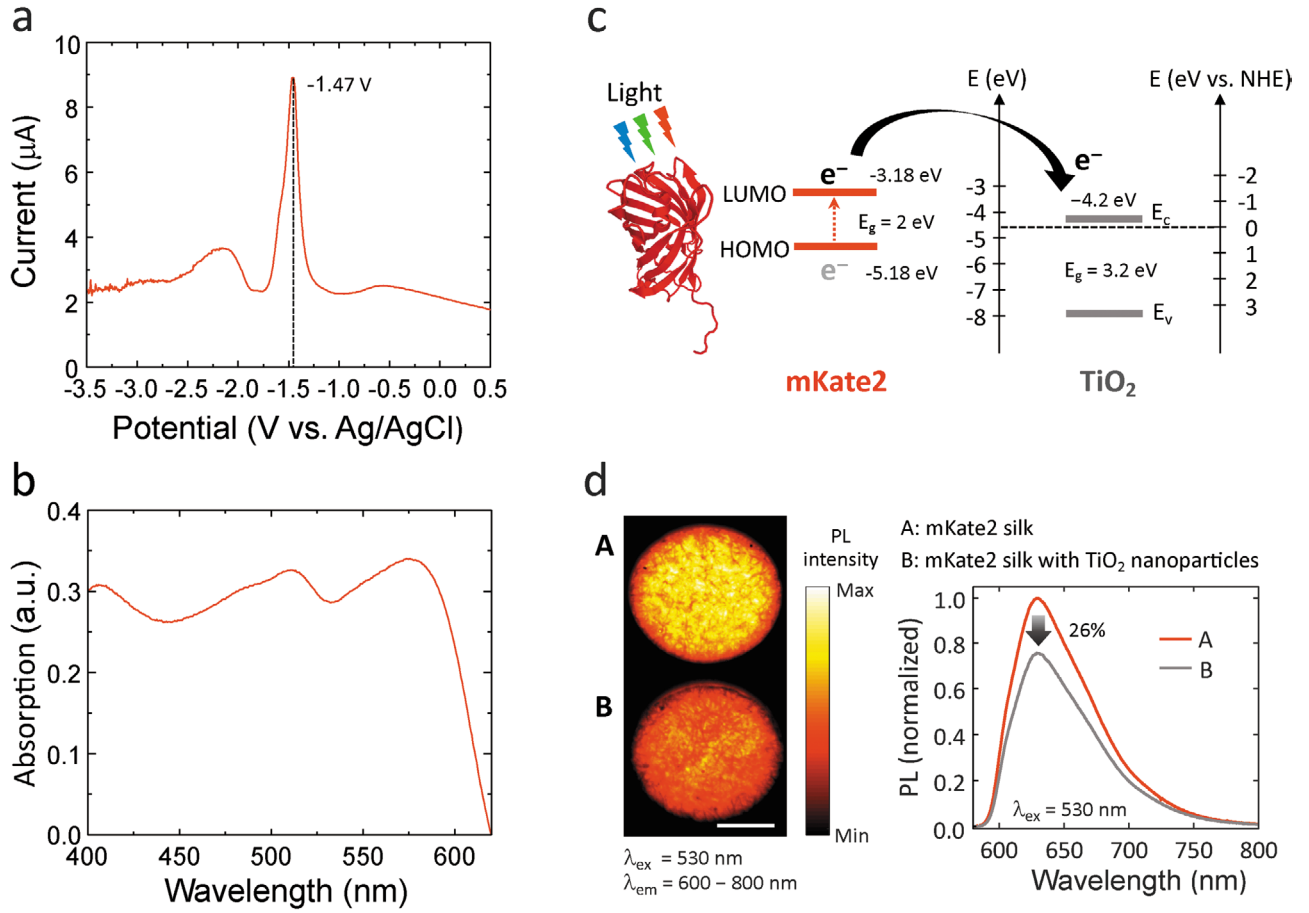

Figure 2. Electrochemical and optical properties of mKate2 silk. a) Square wave voltammetry plot of mKate2 silk measured with reference to the Ag/AgCl reference electrode. The first reduction peak is measured at the potential bias of -1.47 V. b) Absorption spectrum of mKate2 silk. c) Bandgap structure and redox potential of mKate2 silk and electron transfer mechanism between mKate2 silk and TiO_2. LUMO: lowest unoccupied molecular orbital. HOMO: highest occupied molecular orbital. E_g: energy bandgap. E_c: conduction band. E_v: valance band. d) Photoluminescence (PL) images (λ_{em} = 600–800 nm) and spectra of bare mKate2 silk and mKate2 silk coated with TiO_2 nanoparticles at an excitation of λ_{ex} = 530 nm. PL quenching of mKate2 silk indicates electron transfer from mKate2 to TiO_2. The scale bar is 0.2 cm.

2.3. Photoelectric Conversion Characterizations of mKate2 Silk

To test the photoelectric conversion property of mKate2 silk in the visible wavelength range, we fabricate a simple measurement testing device (Figure S2, Supporting Information) and conduct a series of in situ photoelectric measurements.[24] By measuring the short-circuit current density (J_{sc}) and the open-circuit voltage (V_{oc}), we quantify the time-resolved switching behavior of mKate2 silk (**Figure 3**a). Repeated visible light illumination with on and off is applied at different central wavelengths of λ = 470, 530, 565, and 625 nm with the optical intensity of 14 mW cm^{-2} (see Experimental Section). Figure 3a clearly shows that both J_{sc} and V_{oc} photogenerated by mKate2 silk are reproducibly switched from the "high" state to the "low" state by periodically turning each light source on and off. This result supports the idea that the electrons photogenerated by mKate2 silk are transferred to the anode electrode (i.e., TiO_2 layer), owing to the higher LUMO level than the conduction band of TiO_2 (Figure 2c). The decaying pattern with the increase in λ is also in excellent agreement with the absorption spectrum of the mKate2 silk device (Figure S3, Supporting Information). We further evaluate a photoresponsivity (R) and a light on/off ratio in a self-power mode without applying external power to the device at zero bias (i.e., 0 V) (Figure 3b). The highest photoresponsivity ($R = J/P$) of 1.103 mA W^{-1} and light on/off ratio (J_{light}/J_{dark}) of 2.574×10^3 are obtained at λ = 470 nm with the optical intensity of 14 mW cm^{-2}, where the photocurrent density J is determined by $J = J_{light} - J_{dark}$ (J_{light} = 15.443 ± 0.012 μA cm^{-2} and J_{dark} = 0.006 ± 0.004 μA cm^{-2}) and P is the incident light intensity (i.e., 14 mW cm^{-2}).

To factor out contributions from the electrolyte and the natural silk compositions, we separately test two different devices, consisting of the electrolyte without any silk and with white silk (*Bombyx mori*) only under the same experimental conditions, respectively (Figure S4, Supporting Information). Because the electrolyte consisting of triiodide/iodide (I_3^-/I^-) partially absorbs the visible light, dominantly in λ < 480 nm,[25] the device without any silk still shows the time-resolved switching behavior. However, J_{sc} and V_{oc} values are very low as J_{sc} = 5.642 ± 0.017 μA cm^{-2} and V_{oc} = 0.167 ± 0.001 V at λ = 470 nm with 14 mW cm^{-2}, respectively (Figure S4a, Supporting Information). Compared to the electrolyte one, the device with white

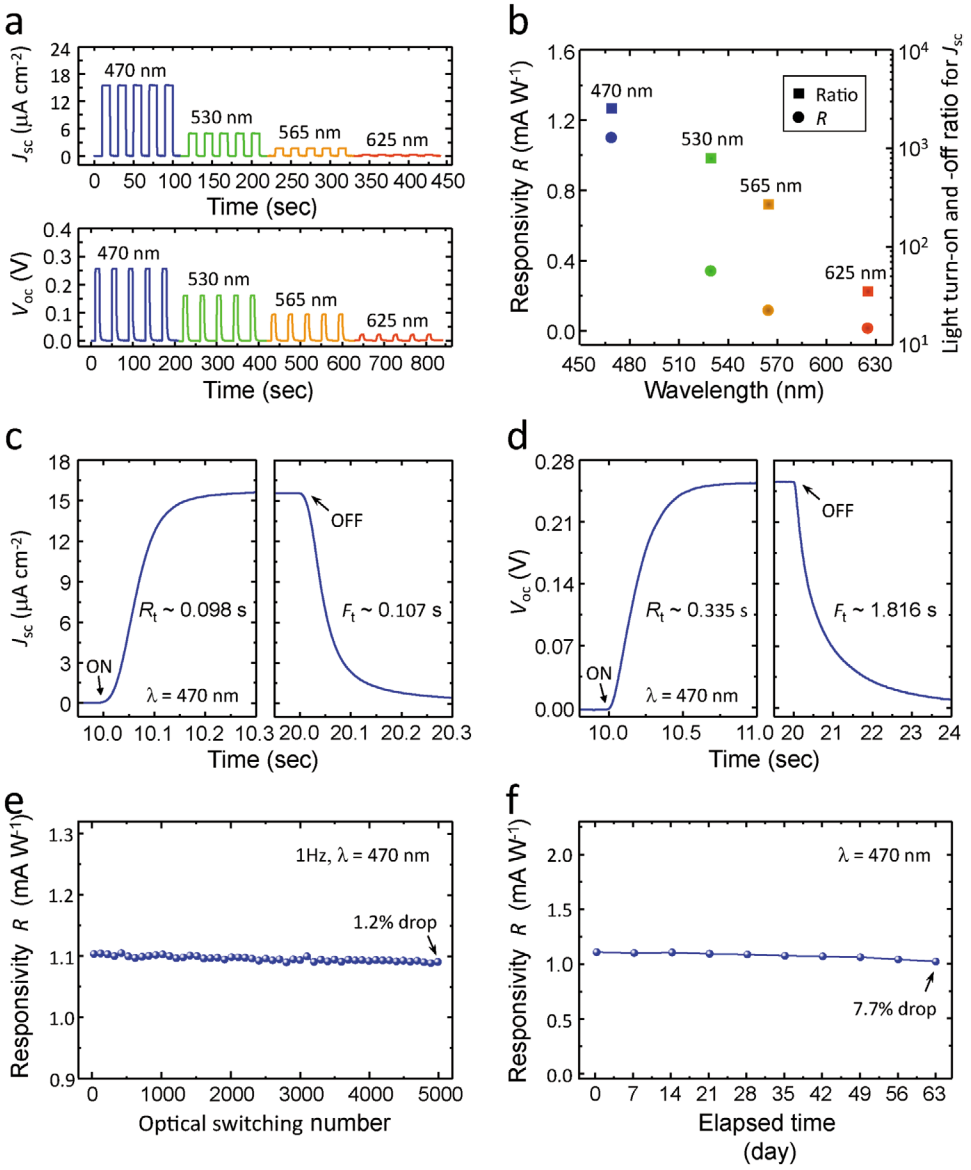

Figure 3. Photoelectric conversion characteristics of mKate2 silk in the visible range. a) Time-resolved photoresponses on the short-circuit current density (J_{sc}) and the open-circuit voltage (V_{oc}) measured for the light-on and -off states upon light illumination at λ = 470, 530, 565 nm, and 625 nm with the optical intensity of 14 mW cm^{-2}. b) Photoresponsivity R (circle) and light turn-on/-off ratio (square) on J_{sc} and V_{oc} for the corresponding light illumination. Rising and falling edges zoomed to estimate the rise time R_t and the fall time F_t for c) J_{sc} and d) V_{oc} at λ = 470 nm (optical intensity = 14 mW cm^{-2}). e) Photoresponsivity R of optical switching on J_{sc} upon the light-on and -off states (1 Hz, λ = 470 nm, and 14 mW cm^{-2}) as a function of the on/off optical switching number. f) Long-term stability under the laboratory conditions (22 ± 2 °C and 40–50% relative humidity).

silk (without mKate2) shows slightly higher J_{sc} and V_{oc} values of 8.386 ± 0.022 μA cm^{-2} and 0.178 ± 0.001 V at λ = 470 nm with 14 mW cm^{-2}, respectively (Figure S4b, Supporting Information). This enhancement for natural silk (without mKate2) can be ascribable to the strong light scattering of silk fiber structures.[7] This result can also be understood by the fact that additional ionic charge carriers in natural silk, caused by the presence of ionic elements (i.e., Na, Cl, K, etc.) in white silk (*Bombyx mori*), facilitate electron transport with electrolyte ions (i.e., I_3^-/I^-).[6,21] In other words, the current flowing property in mKate2 silk fibers can be attributable to the migration of ionic charge carriers, such as Ca, Na, Mg, K, and Cl (Table S1, Supporting Information),[6] circulating the electrons in the whole device. More importantly, these results show that mKate2 plays a dominant role in the generation of photoinduced electrons, mainly contributing to the photoelectric conversion performance.

We also characterize the response speed of mKate2 silk from the temporal photoresponse curves. The response speed is extracted by determining the rise time R_t and the fall time F_t, respectively (Figure 3c,d); R_t is defined as a time interval to rise from 10% to 90% of its peak value, while F_t is defined as a time interval to decay from 90% to 10% of its peak value. A relatively rapid photoresponse speed is observed for J_{sc}, while a slow photoresponse with much longer R_t and F_t is shown

for V_{oc}. Specifically, under the blue light illumination (λ = 470 nm and optical intensity = 14 mW cm^{-2}), R_t and F_t values are ≈0.098 and ≈0.107 second for J_{sc} (15.443 ± 0.012 μA cm^{-2}), ≈0.335 and ≈1.816 second for V_{oc} (0.256 ± 0.001 V), respectively. For V_{oc}, these characteristics indicate a slow recombination rate of photogenerated electrons by the electrolyte ions at the TiO_2/electrolyte interface, because there is no current passing through the external circuit.[26] We also evaluate the temporal stability of mKate2 silk, because almost all fluorescent molecules are subject to photobleaching.[12a,12b] The photostability of real-time J_{sc} responses is tested by periodically switching the illumination signal (λ = 470 nm and optical intensity = 14 mW cm^{-2}) on and off with a frequency of 1 Hz (Figure S5, Supporting Information). Figure 3e shows a reproducible and stable photoresponse between light on- and off-states. Even after optical switching cycles of 5000, the photoresponsivity (R) is reached to be 1.09 mA W^{-1}, but the relative decrease is only 1.2% compared to its initial R = 1.103 mA W^{-1}. The long-term stability of mKate2 silk is further examined for an extended period of 63 d (the device was stored in the laboratory under the dark ambient conditions of 22 ± 2 °C and 40–50% relative humidity). Figure 3f reveals that the photocurrent is significantly retained with a reduction percentage of ≈7.7% only with R = 1.018 mA W^{-1}. Indeed, mKate2 silk is stable even when contacted with TiO_2 and the electrolyte for the extended period of time.

2.4. Bioassisted Plasmonic TiN-Hybridized mKate2 Silk Production

One common approach for enhancing the light coupling and absorption in optoelectronic devices is to incorporate plasmonics, in which a plasmonic enhancement requires spatial and spectral arrangements.[22a,27] First, the distance between a plasmonic nanoparticle and a fluorophore should be within the spatial extent of the plasmonic hot field, which is typically less than 5–100 nm.[27c,28] A simple coating of plasmonic nanoparticles or nanomaterials on the surface of mKate2 silk fibers (diameter ≈ 10–20 μm) has a fundamental limitation, given that a larger amount of mKate2 exists inside silk fibers as a part of the protein sequences.[12d,17c] Thus, bioassisted direct feeding of nanoparticles of interests allows for nanomaterial hybridization inside the silk glands, resulting in nanomaterial-embedded silk fibers via the silkworm's spinning process.[18–19,29] Second, to fully utilize the broad absorption band (λ = 400–620 nm) of mKate2 silk (Figure 2b), the plasmonic resonance band should be spectrally overlapped, which requires metal nanoparticles with large sizes of >50 nm when conventional noble metals such as gold and silver are used.[30] This poses a challenge for bioassisted direct feeding, because the diffusion of large-sized nanoparticles is limited in the open circulatory system of silkworms.[18] To overcome the size limitation, we turn to TiN nanoparticles that satisfy the key plasmonic conditions (e.g., negative permittivity).[31] Importantly, TiN nanoparticles only with an average size of 20 nm have a broad absorption band, covering the entire visible region of 400–700 nm (Figure S6, Supporting Information). As an alternative plasmonic material for replacing expensive noble metals, TiN has recently received considerable attention, including additional advantages of low cost, high thermal/oxidative stability, and even biocompatibility.[31,32]

Figure 4a,b shows TiN-hybridized mKate2 silk cocoons via direct feeding of modified diets, using mulberry leaves immersed in a 0.5% (w v^{-1}) suspension of TiN nanoparticles (see Experimental Section). TiN-hybridized mKate2 silk emits stronger red fluorescent emission (λ_{em} = 600–750 nm) with a PL enhancement percentage of 12.1% at the maximum emission peak of 633 nm, upon green light excitation at λ_{ex} = 530 nm (Figure S7, Supporting Information). The devices constructed with TiN-hybridized mKate2 silk show similar trends in the absorption and the enhancement ratio (Figure S8, Supporting Information). To verify the presence of TiN nanoparticles inside mKate2 silk fibers, we use an energy dispersive X-ray (EDX) analysis (Figure 4c and Figure S9, Supporting Information). In TiN-hybridized mKate2 silk, titanium (Ti) is clearly detected with 0.20 ± 0.10 (mean ± standard deviation) weight percent (wt%) on the fiber surface and 0.18 ± 0.07 wt% inside the cross section, respectively (Table S2, Supporting Information), in addition to the main three elements (i.e., C, O, and N) and other minor elements (i.e., Ca, Na, Mg, K, S, and Cl) (Tables S1 and S2, Supporting Information). We further confirm the presence of TiN inside silk fiber using a Raman analysis (Figure 4d). In general, the strong emission intensity of mKate2 silk completely masks the original Raman scattering signals of silk. Thus, we use TiN-hybridized white silk in the absence of mKate2 produced by natural silkworms (*Bombyx mori*) fed with the same modified diets under the same rearing processes. More importantly, TiN-hybridized silk shows the enhanced Raman intensity at 1085, 1231, 1668, and 2932 cm^{-1} that correspond to the main proteins in *Bombyx mori* silk,[33] as the absorption enhancement band of TiN is close to the excitation wavelength (i.e., λ = 532 nm) (Figure S7b, Supporting Information). It should be noted that this bioassisted TiN hybridization does not significantly affect the fundamental mechanical properties of the resultant silk fibers (p-value of 0.26 in an ANOVA test for comparing the Young's moduli among bare mKate2 silk, TiN-hybridized mKate2 silk, and wild-type white silk) (Table S3 and Figure S10, Supporting Information).

2.5. Photoelectric Conversion Characterizations of TiN-Hybridized mKate2 Silk

Owing to the unique TiN plasmonic effects, the biological hybridization of TiN with mKate2 silk results in improved performance with an overall enhancement factor of about 1.9 at 470 nm in photoresponsivity (Figure S11, Supporting Information). The current density–voltage (J–V) curve of TiN-hybridized mKate2 silk shows the enhanced photoelectric conversion property under the illumination at λ = 470 nm with the optical intensity of 14 mW cm^{-2} (**Figure 5**a). Clearly, J_{sc} and V_{oc} are higher values with J_{sc} = 29.306 ± 0.035 μA cm^{-2} and V_{oc} = 0.390 ± 0.001 V, compared to bare mKate2 silk (J_{sc} = 15.443 ± 0.012 μA cm^{-2} and V_{oc} = 0.256 ± 0.001 V), respectively. In addition, both of R and the light turn-on/-off ratio are considerably enhanced to be 2.093 mA W^{-1} and 5.861 × 10^3,

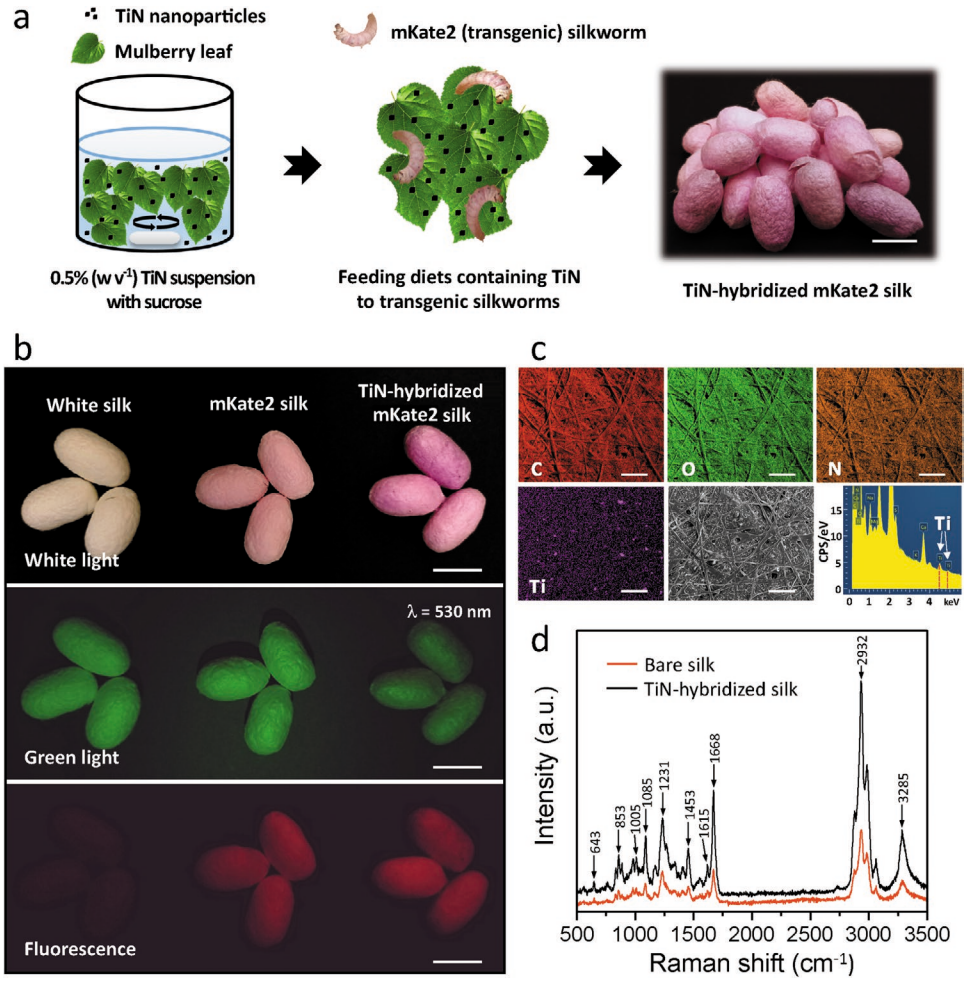

Figure 4. Biological hybridization of titanium nitride (TiN) nanoparticles with mKate2 silk. a) Schematic diagram of the biological hybridization of TiN nanoparticles (average size of 20 nm) with mKate2 silk by direct feeding of modified diets, i.e., mulberry leaves immersed in a 0.5% (w v^{-1}) TiN suspension with 4% (w v^{-1}) sucrose, to mKate2 (transgenic) silkworms. The scale bar is 2 cm. b) Photographs of white silk cocoons and mKate2 (transgenic) silk cocoons with and without TiN nanoparticles. Upon the green light excitation (λ_{ex} = 530 nm), the fluorescent image (λ = 600–800 nm) of TiN-hybridized mKate2silk shows a higher intensity than that of mKate2 silk. The scale bars are 2 cm. c) Energy-dispersive X-ray spectroscopy (EDX) elemental mapping images and spectrum on the surface of TiN-hybridized mKate2 silk and its corresponding SEM image. The EDX results show that silk contains the main three elements of carbon (C), oxygen (O), and nitrogen (N), including other minor elements of calcium (Ca), sodium (Na), magnesium (Mg), potassium (K), sulfur (S), and chlorine (Cl). Note that TiN-hybridized mKate2 silk contains the element of titanium (Ti). The scale bars are 200 µm. d) Plasmon-enhanced Raman spectrum of TiN-hybridized white silk upon the excitation at λ_{ex} = 532 nm, compared to bare white silk.

respectively (J_{dark} = 0.005 ± 0.004 µA cm^{-2}). In Figure 5b, J_{sc} and V_{oc} of mKate2 silk with and without TiN are further analyzed as a function of the incident optical intensity under illumination at λ = 470 nm. For TiN-hybridized mKate2 silk, J_{sc} covers a wider range up to ≈68 µA cm^{-2}, linearly increasing with the light intensity from 2 to 30 mW cm^{-2}. On the other hand, V_{oc} rises rapidly at low optical intensity (2–10 mW cm^{-2}) followed by a plateau at the optical intensity above 10 mW cm^{-2}, due to the proportional relationship of V_{oc} and $\ln(J_{light}/J_{dark})$. In Figure 5c, TiN-hybridized mKate2 silk also exhibits reliable time-resolved switching behavior for J_{sc} signals (i.e., self-power mode) upon visible light illumination on and off for different central wavelengths of 470, 530, 565, and 625 nm with the optical intensity of 14 mW cm^{-2}. J_{sc} of TiN-hybridized mKate2 silk has the rise time R_t of ≈0.092 s and the fall time F_t of ≈0.111 s, comparable to those of bare mKate2 silk (Figure 5d). Finally, TiN-hybridized mKate2 silk demonstrates reliably reproducible and stable photoresponsivity between the light on- and off-states after optical switching cycles of 5000 and 63 d with low degradation percentages of 1.4% and 9%, respectively (Figure 5e; Figure S12, Supporting Information).

2.6. Outlook

The reported photoelectric silk can provide an ab initio foundation for opening up largely unexplored opportunities for utilizing biologically derived natural biocompatible or implantable photoelectric materials. Numerous medical and biological applications, such as biosensing, retina prosthesis, artificial photoreceptors, neurostimulation, and optogenetics,

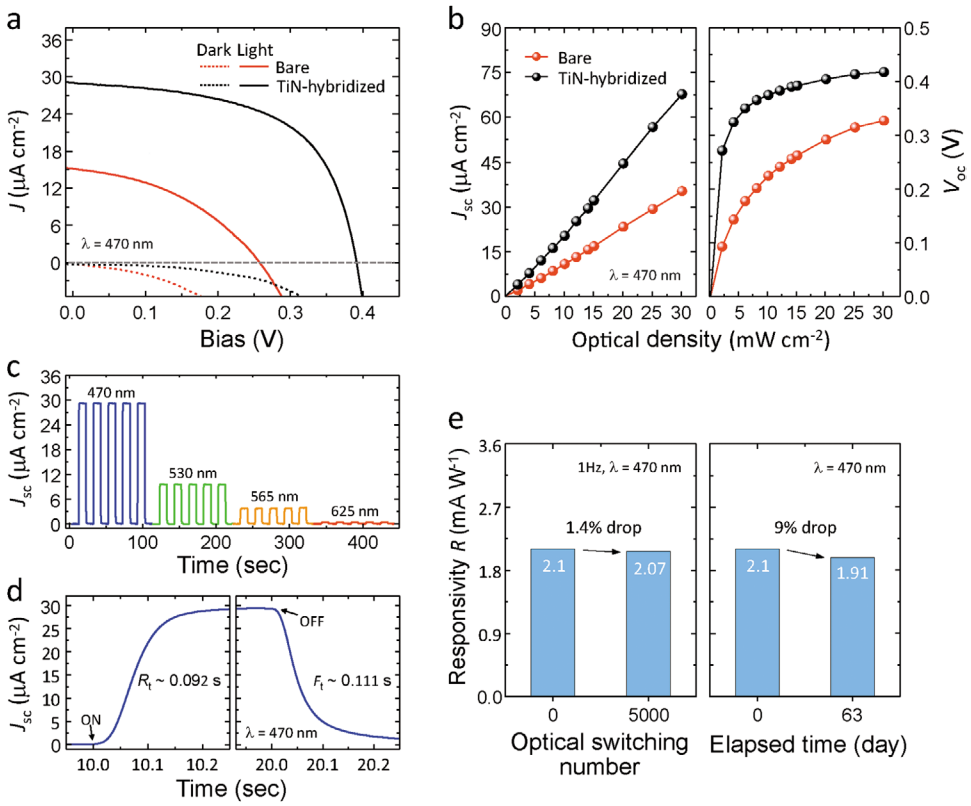

Figure 5. Bioassisted plasmon-enhanced photoelectric conversion characteristics of TiN-hybridized mKate2 silk in the visible range. a) Current density–voltage (*J*–*V*) curves of bare mKate2 silk and TiN-hybridized mKate2 silk under blue light illumination of $\lambda = 470$ nm. b) Short-circuit current density (J_{sc}) and open-circuit voltage (V_{oc}) of bare mKate2 silk and TiN-hybridized mKate2 silk as a function of the optical intensity under blue light illumination of $\lambda = 470$ nm. c) Time response of J_{sc} measured for light turn-on/-off states for TiN-hybridized mKate2 silk under visible light illuminations at $\lambda = 470$, 530, 565, and 625 nm with the optical intensity of 14 mW cm^{-2}. d) Rising and falling edges zoomed to estimate the rise time R_t and the fall time F_t for J_{sc} at $\lambda = 470$ nm (14 mW cm^{-2}). e) Optical switching response on J_{sc} under the light-on and -off states (1 Hz, $\lambda = 470$ nm, and 14 mW cm^{-2}) after an on/off optical switching number of 5000 and long-term stability under the laboratory conditions (22 ± 2 °C and 40–50% relative humidity).

require biocompatible photoelectric materials that convert light to electricity. Although photosensitive receptor proteins and 2D materials have been intensively studied, biologically friendly materials are still limited. Silk itself has biocompatibility, biodegradability, and low immunogenicity. Fluorescent silk does not cause additional toxicity to a biological system as tested in cell viability assessments (Figure S13, Supporting Information). As future development and research enhance the overall photoelectric conversion ability of photoelectric silk comparable to conventional optoelectronic materials, the key advantage that photoelectric silk can potentially provide with biosensors, photoreceptors, and neurostimulators is to minimize material toxicity, tissue reaction, and inflammatory response.

3. Conclusion

We report that mKate2 silk is a biologically derived natural photoelectric biosystem. The genetic hybridization of mKate2 and silk can potentially provide additional advantages originating from the unique physical and biological properties of silk as well as scalable and ecofriendly production using silkworms (i.e., biogenic bioreactor). A fluorescent protein with electron transfer is used as a photoelectric protein. Silk serves a host material as silk proteins have the excellent biocompatible and physical properties. The bioassisted plasmonic functionalization further enhances the light sensing performance in the broad visible wavelength range. Overall, the reported photoelectric silk may offer an alternative protein-based strategy to broaden our material choices to facilitate future bioelectronics device development.

4. Experimental Section

Transformation Vector Construction for Silkworm Transgenesis: Using germline transformation (i.e., *piggyBac* transposon), the transformation vector (p3xP3-EGFP-pFibH-mKate2) was constructed as a *piggyBac*-derived vector and then injected it with a helper vector into preblastoderm embryos.[12d,17a,17b] To obtain the fibroin promoter, the DNA fragment (GenBank Accession No. AF226688, nucleotides 61312-63870) including pFibH promoter domain (1124 bp), N-terminal region 1 (NTR-1, 142 bp), first intron (871 bp), and N-terminal region 2 (NTR-2, 417 bp) was amplified by polymerase chain reaction (PCR) using the genomic DNA from *Bombyx mori* and specific primers (pFibHN-F: 5′-GGCGCGCCGTGCGTGATCAGGAAAAAT-3′ and pFibHN-R: 5′-TGCACCGACTGCAGCACTAGTGCTGAA-3′), followed by treatments

with the restriction enzymes of *Asc*I/*Not*I. The resultant DNA fragment was cloned into pGEM-T Easy Vector System (Promega, Co), named as pGEMT-pFibH-NTR. The DNA fragment (GenBank Accession No. AF226688, nucleotides 79021-79500) including C-terminal region (179 bp, CTR) and poly(A) signal region (301 bp) of the heavy chain was amplified by PCR using genomic DNA from *Bombyx mori* and specific primers (pFibHC-F: 5′- CCTGCAGGAAGTCGACAGCGTCAGTTACGGAGCTGGCAGGGGA-3′ and pFibHC-R: 5′- GGCCGGCC TATAGTATTCTTAGTTGAGAAGGCATA-3′) and then the resultant DNA fragment was cloned into pGEM-T Easy Vector System with the restriction enzymes of *Sal*I/*Sbf*I/*Fse*I, named as pGEMT-CTR. These two fragments were cloned with pBluescriptII SK(-) (Stratagene, CA) digested with *Apa*I/*Sal*I, creating pFibHNC-null. The mKate2 gene was synthesized from BIONEER Co., and then it was cloned into pGEM-T Easy Vector System pGEMT-mKate2 (720 bp). N- and C-terminal had the *Not*I and *Sbf*I restriction sites, respectively. The mKate2 cDNA was digested with *Not*I/*Sbf*I and was subcloned into a pFibHNC-null digested with *Not*I/*Sbf*I, resulting in pFibHNC-mKate2. The pFibHNC-mKate2 vector was digested with *Asc*I/*Fse*I and was subcloned into *pBac*-3xP3-EGFP. The final resultant vector was named as p3xP3-EGFP-pFibH-mKate2.

Bioassisted Hybridization of Titanium Nitride (TiN) with mKate2 Silk: Modified diets were fed containing TiN nanoparticles to transgenic silkworms as follows: A uniformly dispersive solution with a concentration of 0.5% (w v^{-1}) TiN nanoparticles (size ≈ 20 nm) was prepared in deionized water including 4% (w v^{-1}) sucrose. Fresh mulberry leaves were soaked into the TiN suspension for five minutes and then placed in a cool place to be dried before feeding each day. mKate2 (transgenic) silkworm larvae were raised with normal diets (i.e., fresh mulberry leaves) from their hatch to the first day of their fifth instar. Healthy and active larvae were randomly selected and were divided into two groups of 30 larvae. A control group was raised with a normal diet of fresh mulberry leaves. The experimental group was reared with modified diets of fresh mulberry leaves containing TiN nanoparticles until their spinning. The rearing condition was 25 ± 2 °C and 40 ± 10% relative humidity.

Electrochemical Characterizations of mKate2 Silk: Square wave voltammetry was used to characterize the energy level of mKate2 silk. The electrochemical measurement was performed using a standard three-electrode configuration with indium tin oxide on a polyethylene naphthalate substrate as a working electrode, a platinum (Pt) counter electrode, and an silver/silver chloride (Ag/AgCl) (3 M potassium chloride saturated) reference electrode in solution phase containing high performance electrolyte (EL-HPE; Greatcell Solar Ltd.). The photoresponse currents from the electrode were obtained using the potentiostat (CompactStat; Ivium Technologies) controlled by a computer equipped with the IviumSoft software package. The potential bias was swept in a scan range from −3.5 to 0.5 V relative to the reference Ag/AgCl electrode using a pulse amplitude of 100 mV, a scanning frequency of 10 Hz, and a voltage step of 5 mV at room temperature. For square wave voltammetry analyses, a customized template (the same platform of mKate2 silk devices) containing a mKate2 silk sample was used (Figure S1, Supporting Information).

Optical Characterizations of mKate2 Silk: The optical properties were including absorption spectra, reflectance images, and photoluminescence (PL) images/spectra, using a fiber bundle-coupled spectrometer with an integrating sphere and a customized mesoscopic spectrometer/imaging setup. For the PL measurements of mKate2 silk in the presence of titanium dioxide (TiO_2) nanoparticles (anatase phase and size < 25 nm). Punched mKate2 silk cocoon discs with a diameter of 0.5 cm were immersed into a solution containing 0.5% (w v^{-1}) TiO_2 nanoparticles for 5 min with stirring of 400 rpm at room temperature and were followed by rinsing with deionized water and drying for 24 h in dark. To detect the PL emission of mKate2 silk, the samples were placed on a mesoscopic spectrometer-imaging system, in which an excitation source at λ_{ex} = 530 nm and an emission filter with λ_{em} = 600–800 nm were used.

To confirm the presence of TiN nanoparticles in silk fibers, a confocal Raman system (HORIBA Jobin Yvon, XploRA) was used with an excitation laser of 532 nm. For mKate2 silk, the strong fluorescence background signal of mKate2 completely masked Raman signals as expected. Thus, white silk cocoons were used without mKate2, which were obtained by wild-type silkworms (*Bombyx mori*) rearing under the same conditions of mKate2 transgenic silkworms fed with TiN nanoparticles. Using a 100 × and NA = 0.90 objective, the Raman laser spot size was smaller than 1 μm^2. To minimize any thermal damage of silk in the air, all measurements were taken with a relatively low excitation power of 1.5 mW (10% of the maximum power). The spectrometer was calibrated with a silicon substrate at 520 cm^{-1} before the measurements. Spectra were recorded from 500 to 3500 cm^{-1} with a 1.4 cm^{-1} spectral width resolution. Two measurements of 10 s scans were averaged for Raman analyses.

Device Fabrication for Photoelectric Conversion Measurements: To explore the photoelectric conversion property of mKate2 silk, we constructed working prototypes of devices using mKate2 silk as follows: As an electron transport layer, a commercial TiO_2 nanoparticulated paste was coated on the conducting side of fluorine-doped tin oxide (FTO) glasses (1.7 cm × 2.5 cm) using a doctor-blade (tape casting) method. The coated TiO_2 film was sequentially annealed at 120 °C for 15 min at 350 °C for 15 min and at 475 °C for 30 min on a hot plate, resulting in the film thickness of ≈10 µm. After cooling, the annealed films were immersed in an aqueous 15×10^{-3} M titanium(IV) chloride solution at 70 °C for 30 min to improve the physical contact between TiO_2 nanoparticles, followed by a rinse with deionized water. mKate2 silk cocoons were punched into discs with a diameter of 0.6 cm. To ensure firm physical contact with electrodes, the mKate2 silk discs were wet by deionized water and then were flatten in between glass slides by applying mechanical pressure (i.e., ≈5 N) in an oven at 37 °C. The resultant thickness was ≈230 ± 20 µm. An organic solvent-based liquid electrolyte (EL-HPE) was uniformly permeated into the mKate2 silk discs. A Pt-coated FTO glass was used as a counter electrode. For assembly, the electrolyte-containing silk disc was placed between TiO_2 and Pt electrodes and was sealed with a hot-melt Parafilm in a sandwich geometry. After assembling the electrodes, small air pockets could be introduced due to the network porosity of silk cocoons. Thus, the electrolyte solution was additionally injected into the device through predrilled holes on the counter electrode and the openings were sealed with the Parafilm and a thin coverglass.

In Situ Characterizations of Photoelectric Conversion: The current density–voltage (*J*–*V*) characteristics of the fabricated mKate2 silk devices using a programmable source meter (2400, Keithley Instruments Inc.) controlled by a LabView program was measured. Time-resolved photoresponse measurements of the devices were performed using a low-noise current preamplifier (Stanford Research Systems, model: SR570) and a real-time digital oscilloscope (DPO7104, Tektronix) with a 10 GS s^{-1} 1 GHz bandwidth. The photoresponse rise and fall time was defined as the time between 10% and 90% of the maximum photocurrent. For illumination light sources, blue, green, orange, and red light emitting diodes (LEDs; Thorlabs Inc.) with central wavelengths of 470 nm (full width at half maximum; FWHM = 25 nm), 530 nm (FWHM = 33 nm), 565 nm (FWHM = 104 nm), and 625 nm (FWHM = 18 nm) were used. A black mask with a diameter of 0.6 cm (area of 0.283 cm^2) was utilized to ensure an accurate measurement of the incident light. The LED power was tuned by controlling the LED drive current (LEDD1B, Thorlabs Inc.) and was calibrated using a power meter (PM100D, Thorlabs Inc.). All measurements were carried out under a dark ambient condition.

Statistical Analysis: For mechanical and cell viability tests, ANOVA tests were conducted using Stata 14.2 statistical software (College Station, TX, USA). For the cell viability test, the metabolic activity results of silk groups were normalized to those of control groups. Error bars in all data represent standard deviations. The number of samples are presented in the figure legend of each dataset. A level of 5% was considered statistically significant.

Supporting Information

Supporting Information is available from the Wiley Online Library or from the author.

Acknowledgements

J.W.L. and A.E.L.A. contributed equally to this work. This work was supported by the seed grant from Engineering Faculty Conversation on Quantum and Nano in Engineering at Purdue University, the Cooperative Research Program for Agriculture Science & Technology Development (PJ015364) from Rural Development Administration of South Korea, and US Air Force Office of Scientific Research (FA2386-17-1-4072). The authors thank Matthew Therkelsen and Richard Kuhn for the cell viability test.

Conflict of Interest

The authors declare no conflict of interest.

Keywords

biomaterials, far-red fluorescent protein, photoelectric conversion, plasmonic hybridization, silkworm transgenesis

Received: February 3, 2020
Revised: April 22, 2020
Published online: May 27, 2020

[1] a) Y. T. Li, Y. Tian, H. Tian, T. Tu, G. Y. Gou, Q. Wang, Y. C. Qiao, Y. Yang, T. L. Ren, *Sensors* **2018**, *18*, 1368; b) P. Nguyen, M. Meyyappan, S. C. Yiu, *Ophthalmic Res.* **2010**, *44*, 1; c) F. T. Hong, *Mol. Biomol. Electron.* **1994**, *240*, 527; d) Z. B. Guo, D. W. Liang, S. Y. Rao, Y. Xiang, *Nano Energy* **2015**, *11*, 654; e) G. X. Li, F. F. Wang, W. G. Yang, W. X. Wang, G. Y. Li, Y. C. Wang, L. Q. Liu, *Adv. Biosyst.* **2019**, *3*, 1800319.

[2] a) C. Choi, M. K. Choi, S. Y. Liu, M. S. Kim, O. K. Park, C. Im, J. Kim, X. L. Qin, G. J. Lee, K. W. Cho, M. Kim, E. Joh, J. Lee, D. Son, S. H. Kwon, N. L. Jeon, Y. M. Song, N. S. Lu, D. H. Kim, *Nat. Commun.* **2017**, *8*, 1664; b) G. Konstantatos, *Nat. Commun.* **2018**, *9*, 5266; c) M. S. Long, P. Wang, H. H. Fang, W. D. Hu, *Adv. Funct. Mater.* **2019**, *29*, 1803807; d) K. Kostarelos, M. Vincent, C. Hebert, J. A. Garrido, *Adv. Mater.* **2017**, *29*, 1700909.

[3] a) C. Z. Liao, Y. C. Li, S. C. Tjong, *Int. J. Mol. Sci.* **2018**, *19*, 3564; b) W. Z. Teo, E. L. K. Chng, Z. Sofer, M. Pumera, *Chem. - Eur. J.* **2014**, *20*, 9627.

[4] D. A. Dupre, N. Tomycz, D. Whiting, M. Oh, *Pain Pract.* **2018**, *18*, 500.

[5] a) K. Tanaka, N. Kajiyama, K. Ishikura, S. Waga, A. Kikuchi, K. Ohtomo, T. Takagi, S. Mizuno, *Biochim. Biophys. Acta, Protein Struct. Mol. Enzymol.* **1999**, *1432*, 92; b) F. J. Chen, D. Porter, F. Vollrath, *J. R. Soc., Interface* **2012**, *9*, 2299; c) Y. Qi, H. Wang, K. Wei, Y. Yang, R. Y. Zheng, I. S. Kim, K. Q. Zhang, *Int. J. Mol. Sci.* **2017**, *18*, 237.

[6] B. Tulachan, S. K. Meena, R. K. Rai, C. Mallick, T. S. Kusurkar, A. K. Teotia, N. K. Sethy, K. Bhargava, S. Bhattacharya, A. Kumar, R. K. Sharma, N. Sinha, S. K. Singh, M. Das, *Sci. Rep.* **2015**, *4*, 5434.

[7] a) S. H. Choi, S. W. Kim, Z. Ku, M. A. Visbal-Onufrak, S. R. Kim, K. H. Choi, H. Ko, W. Choi, A. M. Urbas, T. W. Goo, Y. L. Kim, *Nat. Commun.* **2018**, *9*, 452; b) N. N. Shi, C. C. Tsai, M. J. Carter, J. Mandal, A. C. Overvig, M. Y. Sfeir, M. Lu, C. L. Craig, G. D. Bernard, Y. Yang, N. F. Yu, *Light: Sci. Appl.* **2018**, *7*, 37.

[8] a) F. Riboli, N. Caselli, S. Vignolini, F. Intonti, K. Vynck, P. Barthelemy, A. Gerardino, L. Balet, L. H. Li, A. Fiore, M. Gurioli, D. S. Wiersma, *Nat. Mater.* **2014**, *13*, 720; b) S. F. Liew, S. M. Popoff, S. W. Sheehan, A. Goetschy, C. A. Schmuttenmaer, A. D. Stone, H. Cao, *ACS Photonics* **2016**, *3*, 449.

[9] a) H. Tao, D. L. Kaplan, F. G. Omenetto, *Adv. Mater.* **2012**, *24*, 2824; b) A. E. Thurber, F. G. Omenetto, D. L. Kaplan, *Biomaterials* **2015**, *71*, 145; c) K. N. Kim, J. Chun, S. A. Chae, C. W. Ahn, I. W. Kim, S. W. Kim, Z. L. Wang, J. M. Baik, *Nano Energy* **2015**, *14*, 87; d) J. W. Leem, M. S. Kim, S. H. Choi, S. R. Kim, S. W. Kim, Y. M. Song, R. J. Young, Y. L. Kim, *Nat. Commun.* **2020**, *11*, 328; e) S. E. V. Yucha, K. A. Tamamoto, H. Nguyen, D. M. Cairns, D. L. Kaplan, *Adv. Biosyst.* **2019**, *3*, 1800283.

[10] J. G. Hardy, L. M. Romer, T. R. Scheibel, *Polymer* **2008**, *49*, 4309.

[11] a) J. W. Leem, S. R. Kim, K. H. Choi, Y. L. Kim, *Nano Convergence* **2018**, *5*, 8; b) A. J. Trewin, B. J. Berry, A. Y. Wei, L. L. Bahr, T. H. Foster, A. P. Wojtovich, *Free Radical Biol. Med.* **2018**, *128*, 157.

[12] a) F. V. Subach, V. V. Verkhusha, *Chem. Rev.* **2012**, *112*, 4308; b) A. Acharya, A. M. Bogdanov, B. L. Grigorenko, K. B. Bravaya, A. V. Nemukhin, K. A. Lukyanov, A. I. Krylov, *Chem. Rev.* **2017**, *117*, 758; c) S. Acikgoz, Y. Ulusu, S. Akin, S. Sonmezoglu, I. Gokce, M. N. Inci, *Ceram. Int.* **2014**, *40*, 2943; d) J. W. Leem, J. Park, S. W. Kim, S. R. Kim, S. H. Choi, K. H. Choi, Y. L. Kim, *Adv. Sci.* **2018**, *5*, 1700863.

[13] M. E. Bulina, K. A. Lukyanov, O. V. Britanova, D. Onichtchouk, S. Lukyanov, D. M. Chudakov, *Nat. Protoc.* **2006**, *1*, 947.

[14] S. Pletnev, N. G. Gurskaya, N. V. Pletneva, K. A. Lukyanov, D. M. Chudakov, V. I. Martynov, V. O. Popov, M. V. Kovalchuk, A. Wlodawer, Z. Dauter, V. Pletnev, *J. Biol. Chem.* **2009**, *284*, 32028.

[15] a) N. Lambert, Y. N. Chen, Y. C. Cheng, C. M. Li, G. Y. Chen, F. Nori, *Nat. Phys.* **2013**, *9*, 10; b) H. B. Xin, W. J. Sim, B. Namgung, Y. Choi, B. J. Li, L. P. Lee, *Nat. Commun.* **2019**, *10*, 3245.

[16] a) K. Deepankumar, A. George, G. K. Priya, M. Ilamaran, N. R. Kamini, T. S. Senthil, S. Easwaramoorthi, N. Ayyadurai, *ACS Sustainable Chem. Eng.* **2017**, *5*, 72; b) Z. G. Chirgwandi, I. Panas, L. G. Johansson, B. Norden, M. Willander, D. Winkler, H. Agren, *J. Phys. Chem. C* **2008**, *112*, 18717; c) L. RandersEichhorn, C. R. Albano, J. Sipior, W. E. Bentley, G. Rao, *Biotechnol. Bioeng.* **1997**, *55*, 921; d) J. W. Choi, Y. S. Nam, W. H. Lee, D. Kim, M. Fujihira, *Appl. Phys. Lett.* **2001**, *79*, 1570; e) A. M. Bogdanov, A. S. Mishin, I. V. Yampolsky, V. V. Belousov, D. M. Chudakov, F. V. Subach, V. V. Verkhusha, S. Lukyanov, K. A. Lukyanov, *Nat. Chem. Biol.* **2009**, *5*, 459.

[17] a) T. Tamura, C. Thilbert, C. Royer, T. Kanda, E. Abraham, M. Kamba, N. Komoto, J. L. Thomas, B. Mauchamp, G. Chavancy, P. Shirk, M. Fraser, J. C. Prudhomme, P. Couble, *Nat. Biotechnol.* **2000**, *18*, 81; b) F. Teule, Y. G. Miao, B. H. Sohn, Y. S. Kim, J. J. Hull, M. J. Fraser, R. V. Lewis, D. L. Jarvis, *Proc. Natl. Acad. Sci. USA* **2012**, *109*, 923; c) T. Iizuka, H. Sezutsu, K. Tatematsu, I. Kobayashi, N. Yonemura, K. Uchino, K. Nakajima, K. Kojima, C. Takabayashi, H. Machii, K. Yamada, H. Kurihara, T. Asakura, Y. Nakazawa, A. Miyawaki, S. Karasawa, H. Kobayashi, J. Yamaguchi, N. Kuwabara, T. Nakamura, K. Yoshii, T. Tamura, *Adv. Funct. Mater.* **2013**, *23*, 5232; d) D. W. Kim, O. J. Lee, S. W. Kim, C. S. Ki, J. R. Chao, H. Yoo, S. I. Yoon, J. E. Lee, Y. R. Park, H. Kweon, K. G. Lee, D. L. Kaplan, C. H. Park, *Biomaterials* **2015**, *70*, 48; e) J. W. Leem, M. J. Fraser, Y. L. Kim, *Annu. Rev. Biomed. Eng.* **2020**, *22*, 79.

[18] R. Xing, X. D. Chen, Y. F. Zhou, J. Zhang, Y. Y. Su, J. F. Qiu, Y. H. Sima, K. Q. Zhang, Y. He, S. Q. Xu, *Sci. Rep.* **2016**, *6*, 19802.

[19] a) Q. Wang, C. Y. Wang, M. C. Zhang, M. Q. Jian, Y. Y. Zhang, *Nano Lett.* **2016**, *16*, 6695; b) L. Y. Cai, H. L. Shao, X. C. Hu, Y. P. Zhang, *ACS Sustainable Chem. Eng.* **2015**, *3*, 2551; c) N. C. Tansil, Y. Li,

C. P. Teng, S. Y. Zhang, K. Y. Win, X. Chen, X. Y. Liu, M. Y. Han, *Adv. Mater.* **2011**, *23*, 1463.

[20] D. Shcherbo, C. S. Murphy, G. V. Ermakova, E. A. Solovieva, T. V. Chepurnykh, A. S. Shcheglov, V. V. Verkhusha, V. Z. Pletnev, K. L. Hazelwood, P. M. Roche, S. Lukyanov, A. G. Zaraisky, M. W. Davidson, D. M. Chudakov, *Biochem. J.* **2009**, *418*, 567.

[21] J. W. Leem, S. H. Choi, S. R. Kim, S. W. Kim, K. H. Choi, Y. L. Kim, *Mater. Horiz.* **2017**, *4*, 281.

[22] a) X. C. Ma, Y. Dai, L. Yu, B. B. Huang, *Light: Sci. Appl.* **2016**, *5*, e16017; b) B. G. Kim, X. Ma, C. Chen, Y. Ie, E. W. Coir, H. Hashemi, Y. Aso, P. F. Green, J. Kieffer, J. Kim, *Adv. Funct. Mater.* **2013**, *23*, 439.

[23] Y. Wu, W. Yang, Y. Fan, Q. H. Song, S. M. Xiao, *Sci. Adv.* **2019**, *5*, eaax0939.

[24] a) J. W. Leem, A. E. Llacsahuanga Allcca, J. J. Chen, S. W. Kim, K. Y. Kim, K. H. Choi, Y. P. Chen, S. R. Kim, Y. L. Kim, *Opt. Express* **2018**, *26*, 31817; b) J. R. Fang, D. Wang, C. T. DeVault, T. F. Chung, Y. P. Chen, A. Boltasseva, V. M. Shalaev, A. V. Kildishev, *Nano Lett.* **2017**, *17*, 57.

[25] J. M. Gardner, M. Abrahamsson, B. H. Farnum, G. J. Meyer, *J. Am. Chem. Soc.* **2009**, *131*, 16206.

[26] X. D. Li, C. T. Gao, H. G. Duan, B. G. Lu, X. J. Pan, E. Q. Xie, *Nano Energy* **2012**, *1*, 640.

[27] a) M. I. Stockman, K. Kneipp, S. I. Bozhevolnyi, S. Saha, A. Dutta, J. Ndukaife, N. Kinsey, H. Reddy, U. Guler, V. M. Shalaev, A. Boltasseva, B. Gholipour, H. N. S. Krishnamoorthy, K. F. MacDonald, C. Soci, N. I. Zheludev, V. Savinov, R. Singh, P. Gross, C. Lienau, M. Vadai, M. L. Solomon, D. R. Barton, M. Lawrence, J. A. Dionne, S. V. Boriskina, R. Esteban, J. Aizpurua, X. Zhang, S. Yang, et al. *J. Opt.* **2018**, *20*, 043001; b) W. Kim, S. H. Lee, J. H. Kim, Y. J. Ahn, Y. H. Kim, J. S. Yu, S. Choi, *ACS Nano* **2018**, *12*, 7100; c) S. H. Choi, B. Kwak, B. Han, Y. L. Kim, *Opt. Express* **2012**, *20*, 16785.

[28] P. Anger, P. Bharadwaj, L. Novotny, *Phys. Rev. Lett.* **2006**, *96*, 113002.

[29] M. Y. Yan, X. H. Ma, Y. J. Yang, X. Wang, W. C. Cheong, Z. H. Chen, X. H. Xu, Y. J. Huang, S. Wang, C. Lian, Y. D. Li, *Nano Lett.* **2018**, *18*, 6017.

[30] a) Z. Starowicz, R. Wojnarowska-Nowak, P. Ozga, E. Sheregii, *Colloid Polym. Sci.* **2018**, *296*, 1029; b) J. Y. Luan, J. J. Morrisse, Z. Y. Wang, H. G. Derami, K. K. Liu, S. S. Cao, Q. S. Jiang, C. Z. Wang, E. D. Kharasch, R. R. Naik, S. Singamaneni, *Light: Sci. Appl.* **2018**, *7*, 29.

[31] U. Guler, S. Suslov, A. V. Kildishev, A. Boltasseva, V. M. Shalaev, *Nanophotonics* **2015**, *4*, 269.

[32] G. K. Hyde, S. D. McCullen, S. Jeon, S. M. Stewart, H. Jeon, E. G. Loboa, G. N. Parsons, *Biomed. Mater.* **2009**, *4*, 025001.

[33] V. Prajzler, K. Min, S. Kim, P. Nekvindova, *Materials* **2018**, *11*, 112.